of these products in the perspective of the upcoming GEO Imaging Satellite (GISAT) missions is also being planned. GISAT is an Indian geo-imaging satellite for providing images quickly during disasters.

1. Gultepe, I. *et al.*, The fog remote sensing and modelling (FRAM) field project and preliminary report. *Bull. Am. Meteorol. Soc.*, 2009, **90**(3), 341–359.
2. Chaurasia, S. and Gohil, B. S., An objective method for detecting night time fog using MODIS data over northern India. *J. Geomat.*, 2016, **10**.
3. Tiwari, S., Payra, S., Mohan, M., Verma, S. and Bhisht, D. S., Visibility degradation during foggy period due to anthropogenic urban aerosol at Delhi, India. *Atmos. Pollut. Res.*, 2011, **2**, 116–120.
4. Mitra, A. K., Sankar Nath and Sharma, A. K., Fog forecasting using rule-based fuzzy inference system. *J. Indian Soc. Remote Sensing*, 2008, **36**(3), 243.
5. Roy Bhowmik, S. K., Sud, A. M. and Singh, C., Forecasting fog over Delhi – an objective method. *MAUSAM-55*, 2004, **2**, 313, 322.
6. Brij Bhusan, Trivedi, H. K. and Bhatia, R. C., On the persistence of fog over northern parts of India. *MAUSAM-54*, 2003, **4**, 851–860.
7. Berndt, E. B., Molthan, A. L., Vaughan, W. W. and Fuell, K. K., Transforming satellite data into weather forecasts. *AGU EOS*, 2017, **98**; https://doi.org/10.1029/2017EO064449.
8. Lensky, I. M. and Rosenfeld, D., Clouds-Aerosols-Precipitation Satellite Analysis Tool (CAPSAT). *Atmos. Chem. Phys.*, 2008, **8**, 6739–6753.
9. Inoue, T., An instantaneous delineation of convective rainfall areas using split window data of NOAA-7 AVHRR. *J. Meteor. Soc. Jpn*, 1987, **65**, 469–481.
10. Lensky, I. M. and Rosenfeld, D., Satellite-based insights into precipitation formation processes in continental and maritime convective clouds at nighttime. *J. Appl. Meteor.*, 2003, **42**, 1227–1233.
11. Lensky, I. M. and Rosenfeld, D., A night rain delineation algorithm for infrared satellite data based on microphysical considerations. *J. Appl. Meteor.*, 2003, **42**, 1218–1226.
12. Eyre, J. R., Brownscombe, J. L. and Allam, R. J., Detection of fog at night using advanced very high resolution radiometer. *Meteorol. Mag.*, 1984, **113**, 266–271.
13. Bader, M. J., Forbes, G. S., Grant, J. R., Lilly, R. B. E. and Waters, J., *Images in Weather Forecasting*, Cambridge University Press, 1995, p. 493.
14. Ellord, G. P., Advances in the detection and analysis of fog at night using GOES multi spectral infrared imagery. *Weather Forecasting*, 1995, **10**, 606–619.
15. Bendix, J., A satellite-based climatology of fog and low-level stratus in Germany and adjacent areas. *Atmos. Res.*, 2002, **64**, 3–18.
16. Bendix, J. and Bachmann, M., A method for detection of fog using AVHRR-imagery of NOAA satellites suitable for operational purposes. *Meteorol. Rund.*, 1991, **43**, 169–178 (in German).
17. Chaurasia, S., Sathiyamoorthy, V., Paul Shukla, B., Simon, B., Joshi, P. C. and Pal, P. K., Night time fog detection using MODIS data over Northern India. *Meteorol. Appl.*, 2011, **8**(4), 483–494.

ACKNOWLEDGMENTS. We thank the Space Applications Center, Ahmedabad team for their technical, software expertise and implementation of RAPID tool at IMDPS, New Delhi. We specially thank C. M. Kistawal, Shri Ghansyam Sanger and Nitesh Kausik for their valuable suggestions while developing 'RAPID'. The first author thanks to I. M. Lensky and D. Rosenfeld for CAPSAT tool information. We appreciate the assistance of the following persons during the course of research: Mr Virendra Singh and S. K. Mukerjee, IMD for data recovery.

Received 21 December 2017; revised accepted 26 March 2018

doi: 10.18520/cs/v115/i7/1358-1366

Analysis of WorldView-2 band importance in tree species classification based on recursive feature elimination

Huaipeng Liu[1,*], Huijun An[2] and Yongxin Zhang[1]

[1]School of Land and Tourism, Luoyang Normal University, Luoyang, Henan Province, 471934, China
[2]College of forestry, Inner Mongolia Agricultural University, Huhhot, Inner Mongolia, 010019, China

In tree species classifications, different spectral bands feature different importance, and the manner of determining the importance of one band is a problem that needs to be solved. In this study, eight bands of the WorldView-2 fusion data were used as information sources, and a recursive feature elimination based on maximum likelihood (MLC-RFE) was used to sort the importance of these bands. According to the results, the importance of the eight bands was sorted as follows (from important to unimportant): near-infrared 2 > red edge > yellow > red > near-infrared 1 > coastal blue > green > blue. The poorest band combination yielded the lowest overall accuracy (OA) and Kappa coefficient (40.9153%; 0.3080), whereas the optimal band combination presented the highest OA and Kappa coefficient (74.5479%; 0.7029), indicating the large difference in accuracies between the optimal and poorest band combinations. Therefore, selecting important bands bears significance in tree species classifications. The MLC-RFE method significantly solved the band selection problem. Thus, this method should be extended to more complex feature selections.

Keywords: Bands importance, maximum likelihood, recursive feature elimination, tree classification, WorldView-2.

TREE species classification based on image remains an unsolved problem, and it is also a hot topic causing concern in researchers[1,2]. Thus far, numerous scholars consider WorldView-2 or WorldView-2 combined with IKONOS, Quickbird, Lidar and other data as data sources to classify tree species. They use classifiers of decision trees, random forests, linear discriminant analysis, partial least squares discriminant analysis, maximum likelihood and support vector machines to distinguish native tree species and other ground types. The overall accuracy (OA) of these classification results is between 82% and 94%, indicating that related studies have acquired better results[3–11]. However, given the lack of sufficient spectral information, mapping forest types and tree species using

*For correspondence. (e-mail: gatestudy@163.com)

Table 1. WorldView-2 band parameters

Band number	Band name	Spatial resolution (m)	Wavelength range (μm)
1	Coastal blue	2.0	0.400–0.450
2	Blue		0.450–0.510
3	Green		0.510–0.580
4	Yellow		0.585–0.625
5	Red		0.630–0.690
6	Red edge		0.706–0.745
7	Near-infrared 1		0.770–0.895
8	Near-infrared 2		0.860–1.040
9	Panchromatic	0.5	0.450–0.800

high-spatial-resolution satellite data has not reached an acceptable level of accuracy. In image classification, poor band combinations may result in a remarkably low classification accuracy, but an optimal band combination can obtain the best classification results. Therefore, to exclude unimportant bands and retain important bands, optimal classification band sets must be obtained; such condition will serve as a meaningful operation for image classification.

WorldView-2 features eight bands. Compared to conventional high-spatial-resolution remote sensing images and in addition to the red, green, blue and near infrared 1 bands, WorldView-2 also contains additional bands, such as coastal blue, yellow, red edge and near infrared 2 bands. These newly added bands may play an important role in tree species classification. However, in the newly added four bands and the traditional four bands, the important and unimportant ones remain unknown. Thus, experiments must be performed to explore this topic. As few people have considered the importance of each band in tree species classification, in this study, the eight multi-spectral bands of WorldView-2 images were used as signal sources. A recursive feature elimination based on maximum likelihood (MLC-RFE) was used to implement recursive filtering of the eight spectral bands after image fusion. The goals were to verify the importance of each band in tree species classification and to provide theory and method support for the selection of bands in tree species classifications.

The data source came from WorldView-2 image of Hohhot city on 31 August 2011, at a panchromatic band spatial resolution of 0.5 m and eight multi-spectral band spatial resolution of 2 m. Table 1 shows the detailed parameters of WorldView-2.

The study area image features latitudinal and longitudinal ranges of 111°39′12.65″–111°44′35.31″E and 40°46′27.57″–40°49′35.04″N respectively. The area of the study location totals 42 sq. km. The data have been calibrated, fused and atmospheric-corrected before use. To reduce the amount of data computation, in the image range, through on-the-spot reconnaissance and field investigation, we selected a rectangular block area with abundant tree species and cut it out from the WorldView-2 image. The small test area image spans an area of 2.45 sq. km. Figure 1 shows the position relationship between the test area image and the panchromatic, multispectral image (RGB753 combination).

The image of the test area at 1 : 2000 was printed and used for field surveys. The results showed the seven primary types of tree species in this area. On this image, we circled sufficient samples for each type of tree species and marked their names. In the laboratory, we selected the samples carefully and ensured training samples and validation samples showed no overlapping and were evenly dispersed within the study area. The training samples and validation samples of each tree species were drawn into the electronic image in the form of region of interests. Table 2 shows the surveyed tree species and their sample selection.

Previous studies[12–17] have shown that recursive feature elimination (RFE) based on some classifiers (including support vector machines and maximum likelihood) can effectively eliminate negative features, which are necessary for accurate classification. Also, positive characteristics will be retained, and important features can be selected to assist in classification. This method starts with an entire feature set to eliminate the least important characteristics by rounds until only certain features remain. Figure 2 illustrates the methodology flow chart.

The steps of this method are as follows: (1) the feature set T contains all characteristics; (2) the training samples (including only the characteristics in the feature set T) are used to train the classifier; (3) overall classification accuracy of $O(i)$ is calculated after deleting characteristic i in the feature set T; (4) the characteristic i corresponding to maximum $O(i)$ is deleted from the feature set $T(T = T - i)$; (5) steps (2) to (4) are repeated until sufficient characteristics have been deleted; (6) Maximum $O(i)$ values are sorted, and the importance of each feature is analysed to obtain the best classification image.

As the speed of maximum likelihood classification is faster than that of support vector machines and is more sensitive in feature changes[17], in this study, we used MLC-RFE to evaluate the importance of WorldView-2 bands. Then, different band combinations could be selected to analyse the accuracy differences of different

Table 2. Information of surveyed tree species and samples

Common names	Scientific names	Type	Leaf phenology	Pixel number of training samples	Precision validation pixels
Weeping willow	*Salix babylonica*	Broad-leaf tree	Deciduous	1107	1228
Pagoda tree	*Sophora japonica*	Broad-leaf tree	Deciduous	1047	1245
Populus bolleana	*Populus alba* var. *Pyramidalis*	Broad-leaf tree	Deciduous	1066	1250
Chinese pine	*Pinus tabuliformis*	Coniferous tree	Evergreen	1064	1218
Qing qian	*Picea meyeri*	Coniferous tree	Evergreen	614	968
Chinese junipers	*Sabina chinensis*	Coniferous tree	Evergreen	1019	1016
Needle juniper	*Juniperus rigida*	Coniferous tree	Evergreen	1047	1149

Figure 1. WorldView-2 and test area images.

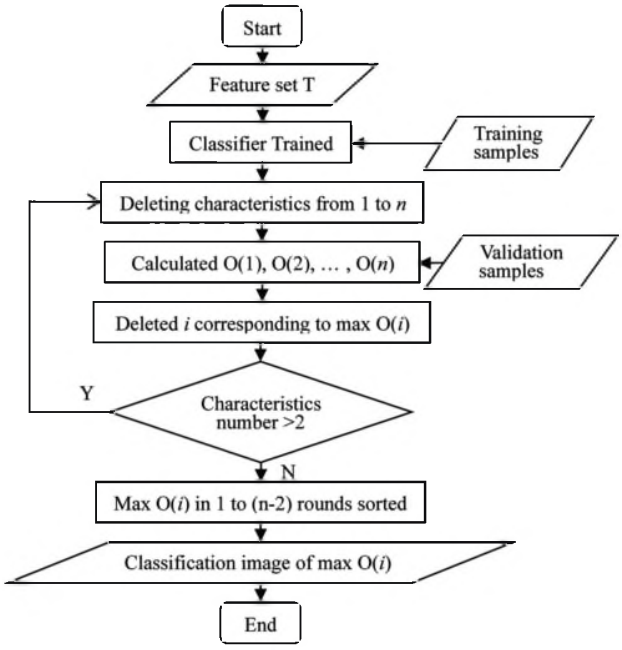

Figure 2. Methodology flow chart.

band combinations in the classification process. Finally, the importance of each band of WorldView-2 could be sorted.

Figure 3 shows the removed bands (grey histogram) and preserved bands (blue histogram) obtained in each round based on MLC-RFE. As shown in Figure 3, in the first round of elimination, we eliminated bands 1–8 of WorldView-2 in order. When band 2 (blue) was eliminated, OA was higher than that of the other eliminated bands. Thus, we assumed that band 2 is unimportant in tree species classification. Then, band 2 was deleted from the feature set. Similarly, in the 2nd to 6th rounds, the green, coastal blue, near-infrared 1, red and yellow bands were eliminated successively.

In the sixth round of elimination, when band 6 was deleted (bands 4 and 8 participated in classification), the OA was 50.7311% (Kappa coefficient was 0.4253). When band 8 was deleted (bands 4 and 6 contributed in classification), OA reached 47.1375% (Kappa coefficient was 0.3833). The classification results of band 4 combined with band 8 were better than those of band 4 combined with band 6, indicating that band 8 is more important than band 6.

The eight bands of WorldView-2 were sorted on importance as follows (from important to unimportant): near-infrared 2 > red edge > yellow > red > near-infrared 1 > coastal blue > green > blue.

Table 3 shows the band eliminated in each round, corresponding OA and kappa coefficients.

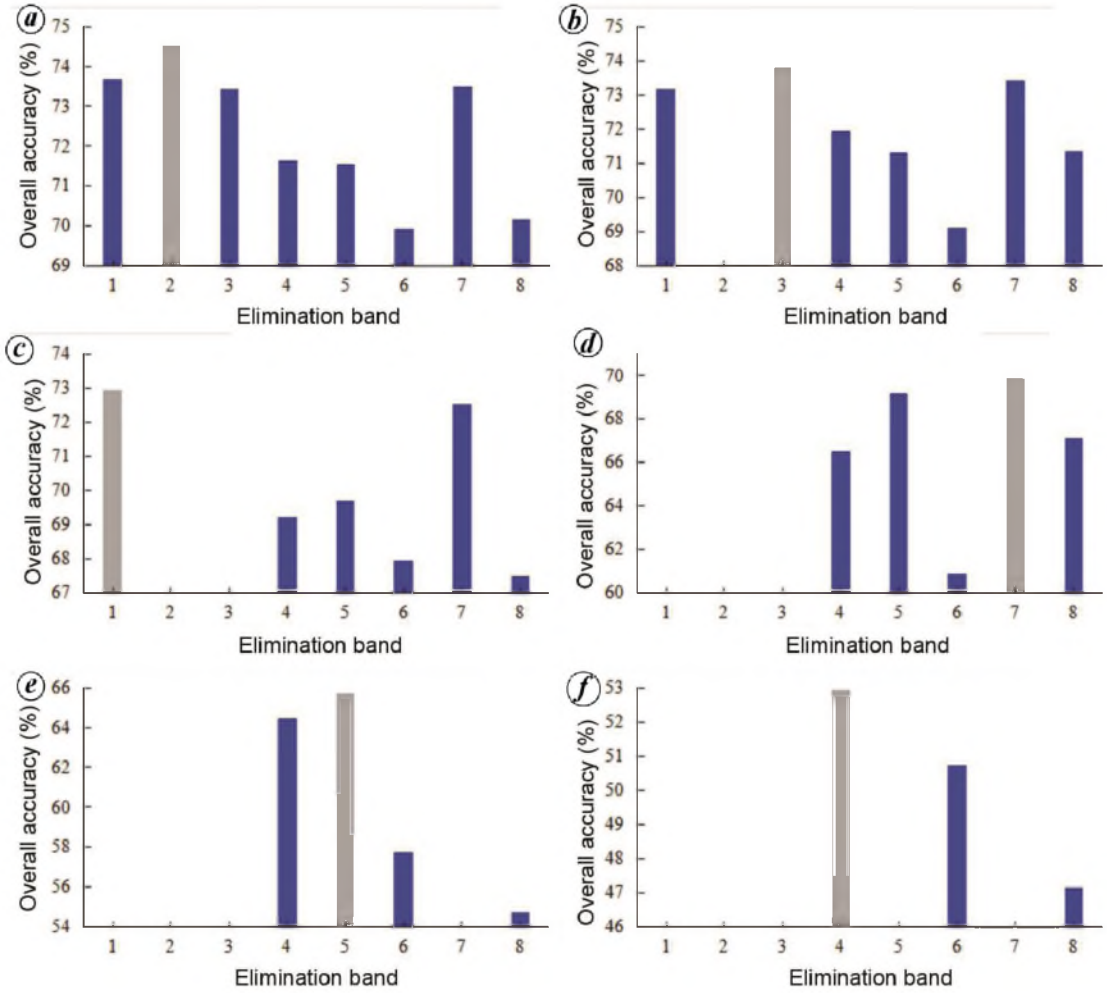

Figure 3. Recursive rounds and band elimination. ***a***, Elimination in the 1st round; ***b***, 2nd round; ***c***, 3rd round; ***d***, 4th round; ***e***, 5th round; ***f***, 6th round.

Table 3. Table of recursive feature elimination

Recursive rounds	Elimination band	Overall accuracy (%)	Kappa coefficient
0	–	74.0713	0.6974
1	Blue	74.5479	0.7029
2	Green	73.8048	0.6941
3	Coastal blue	72.9469	0.6840
4	Near-infrared 1	69.8613	0.6480
5	Red	65.7380	0.5997
6	Yellow	52.9554	0.4501

As presented in Table 3, when all the eight spectral bands were involved in classification (round 0), OA totalled 74.0713% (Kappa coefficient was 0.6974). When the blue band was eliminated in the first round, OA (74.5479%) and Kappa coefficient (0.7029) of the classification reached the highest values, indicating that the blue band is unimportant in tree species classification. With further elimination of the spectral bands, the OA and Kappa coefficient of classification decreased, indicating that the remaining spectral bands are necessary for tree species classification in WorldView-2 images.

Figure 4 shows the recursive elimination rounds of spectral bands and the corresponding OA, 100*Kappa coefficient and 10*(OA – 100*KC).

The Kappa coefficients in Table 3 were multiplied by 100. The OA and 100 times of the Kappa coefficient (KC) curves are compactly shown in the diagram. Correspondingly, the distance between OA and 100 times KC

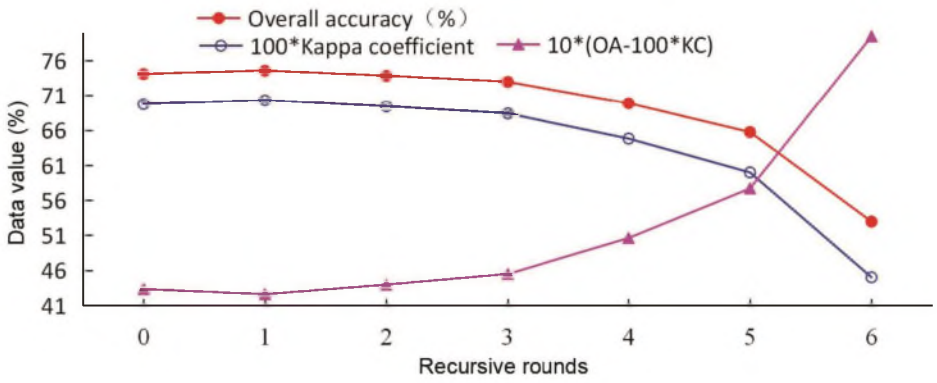

Figure 4. Recursive rounds, corresponding OA, 100* Kappa coefficient and 10* (OA–100*KC).

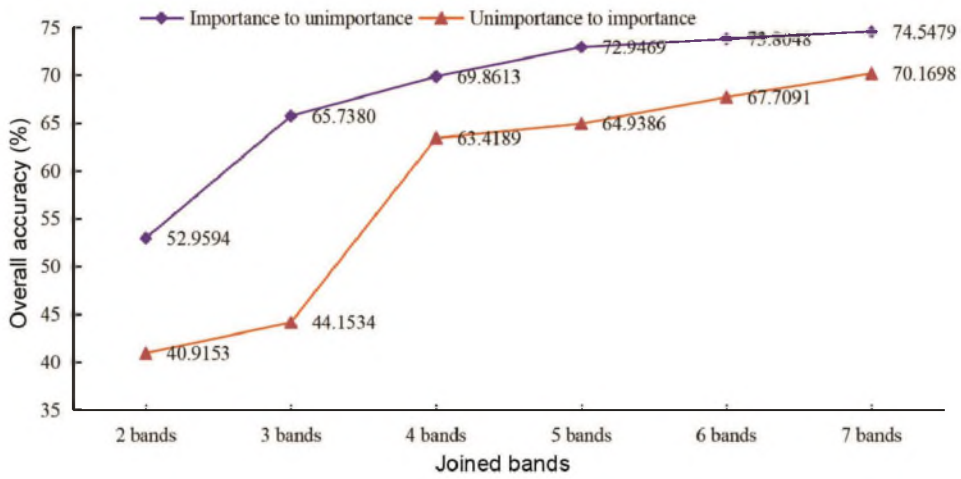

Figure 5. Comparison of curves in important and unimportant band combinations.

Table 4. Band increment classification results

Increasing times	Increase of bands	Overall accuracy %	Kappa coefficient
1	Blue + (green)	40.9153	0.3080
2	Blue + (green + coastal blue)	44.1534	0.3457
3	Blue + (green + coastal blue + near-infrared 1)	63.4189	0.5728
4	Blue + (green + Coastal blue + near-infrared 1 + red)	64.9386	0.5907
5	Blue + (green + Coastal blue + near-infrared 1 + red + yellow)	67.7091	0.6232
6	Blue + (green + Coastal blue + near-infrared 1 + red + yellow + red edge)	70.1698	0.6974

was magnified 10 times, as also shown in the diagram (a purple curve with a triangle).

The distance between the peak of OA and that of the 100*Kappa coefficient is short, indicating that the classification effect is better. Conversely, the classification effect is poor. Figure 3 shows that the distance between the peak of OA and that of the 100*Kappa coefficient was closest in the first round, indicating that the classification effect at that time was the most ideal. From first to sixth rounds, the distance gradually grew, showing that the classification effect progressively worsened.

To further illustrate the importance of band selection in tree species classification, the least important two band combinations were classified after obtaining the sequence of importance of the eight WorldView-2 bands. Then, in accordance with the sequence from unimportant to important, the bands were gradually combined until a combination of seven bands was completed. Table 4 shows the classification results for each band combination.

Table 4 shows that the OA of the blue band combined with the green band (with importance rankings of eighth and seventh) reached 40.9153% (Kappa coefficient was

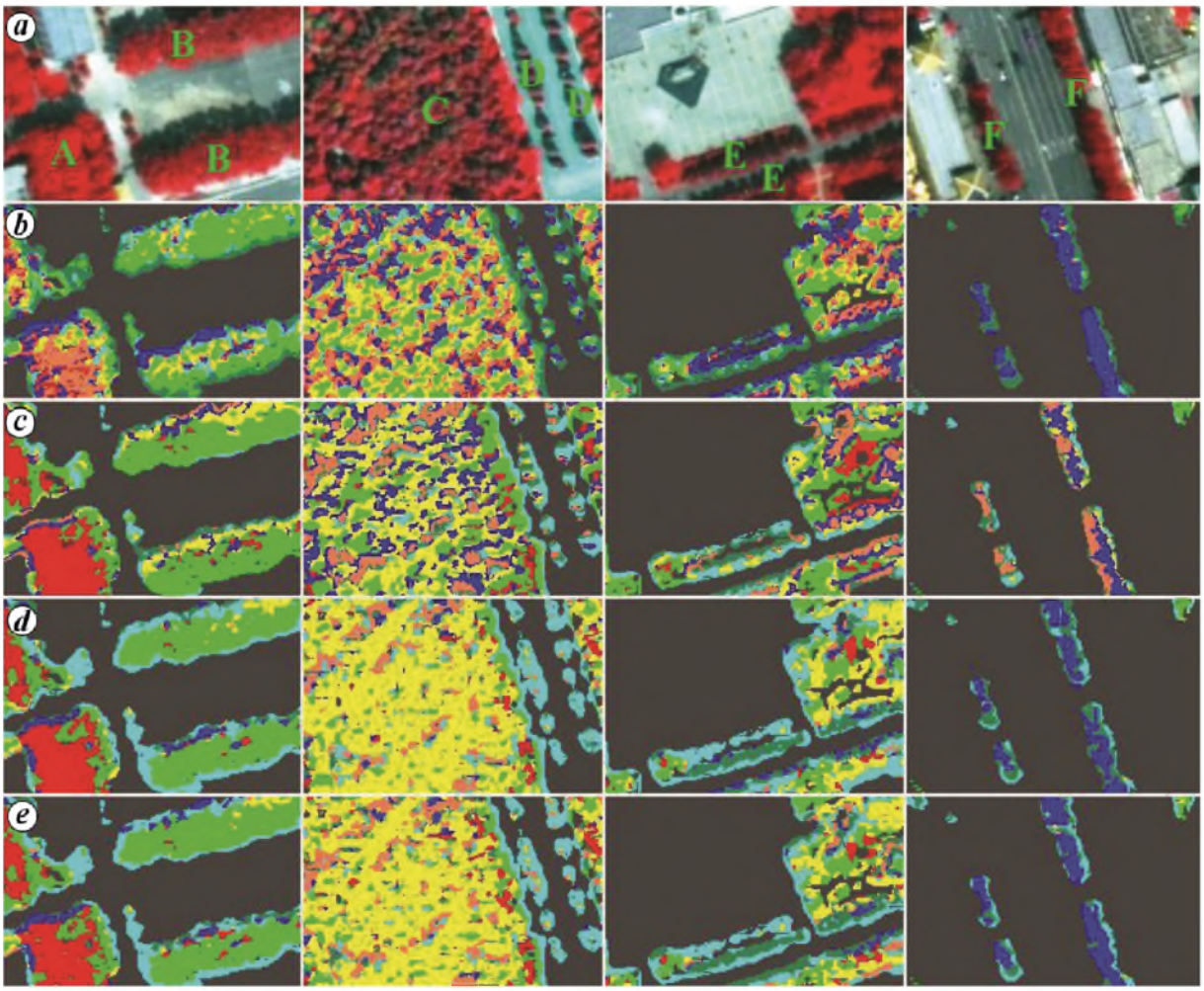

Figure 6. Classification results of representative band combinations.

0.3080). With gradual increase in the importance of spectral bands, the OA and Kappa coefficient of classification gradually increased. The OA of classification totalled 70.1698% (Kappa coefficient was 0.6974) when the seven spectral bands were totally combined.

Figure 5 displays the combination of bands from bands 2 to 7, adoption of the two forms, order from important to unimportant and unimportant to important, and the curves of the two models.

Figure 5 indicates that the OAs in important two-band and seven-band combinations were higher than those in the unimportant two-band and seven-band combinations respectively. The incremental classification results of the eliminated bands ascertained the poorest band combination mode. Correspondingly, the incremental classification results of the important bands ascertained the best band combination mode. Other forms of band combinations produced classification accuracies that will fall into the area enclosed by the two curves.

In this study, four representative cell block images and four representative classification results were selected from the classification results of the different band combinations. Figure 6 shows the classification results. Figure 6 *a* shows the original images (RGB753); Figure 6 *b* displays the classification results of the blue band combined with the green band (the poorest combination of two bands); Figure 6 *c* illustrates the classification results of the red-edge band combined with the near-infrared 2 (the best band combination of two bands); Figure 6 *d* presents the classification results of the coastal blue band combined with the blue, green, yellow, red, red edge and near-infrared 1 bands (poor combination of seven bands); Figure 6 *e* shows the classification results of the coastal blue band combined with the green, yellow, red, red edge, near-infrared 1 and near-infrared 2 bands (the optimal band combination).

In Figure 6 *a*, A, B, C, D, E and F represent *Sophora japonica*, *Salix babylonica*, *Pinus tabuliformis*, *Sabina chinensis*, *Picea meyeri* and *Populus alba* var. *Pyramidalis* respectively.

As shown in Figure 6 *b*, the classification results of *Salix babylonica* and *Populus alba* var. *Pyramidalis* are

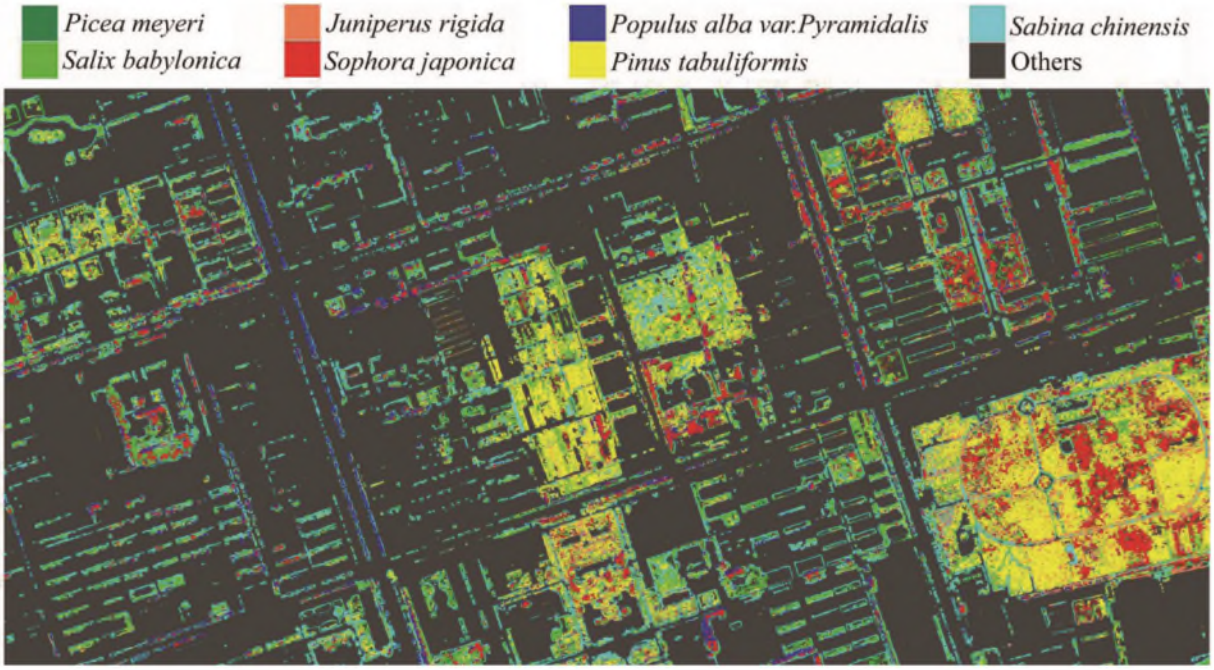

Figure 7. Classification results for the combination of optimal bands.

Table 5. Confusion matrix of the highest OA classification

Tree type	*Salix babylonica*	*Sophora japonica*	*Populus alba* var. *Pyramidalis*	*Pinus tabuliformis*	*Picea meyeri*	*Sabina chinensis*	*Juniperus rigida*	Total row	User accuracy %
Salix babylonica	1053	168	5	88	0	50	0	1364	77.20
Sophora japonica	33	952	53	27	3	8	0	1076	88.48
Populus alba var. *Pyramidalis*	21	107	974	0	86	84	5	1277	76.27
Pinus tabuliformis	39	8	1	973	2	41	60	1124	86.57
Picea meyeri	1	3	139	13	680	249	27	1112	61.15
Sabina chinensis	81	7	57	62	175	523	193	1098	47.63
Juniperus rigida	0	0	21	55	22	61	864	1023	84.46
Total column	1228	1245	1250	1218	968	1016	1149	8074	
Producer accuracy %	85.75	76.47	77.92	79.89	70.25	51.48	75.20		
Overall Accuracy = (6019/8074) = 74.5479%; Kappa Coefficient = 0.7029									

better than those of the other tree species. However, the other tree species showed a serious mixing phenomenon. Therefore, the classification results were remarkably poor. In Figure 6 *c*, the classification results of *Sophora japonica* and *Salix babylonica* are better than those of the other tree species. A serious mixing phenomenon was also observed in these tree species. Thus, the classification results were not ideal. The classification results of Figure 6 *d* and *e* are much better than those of the first two classifications, and a certain but unremarkable difference was observed between the two images. Figure 6 *d*, the classification results of *Populus alba* var. *Pyramidalis* were worse than those in Figure 6 *e*, but *Sophora japonica* yielded the reverse findings.

Figure 7 shows the optimal band combination classification results, and Table 5 lists the confusion matrix of these band classifications.

As presented in Figure 7, recognition of *Populus alba* var. *Pyramidalis* on roads, *Sophora japonica* in arboretum and *Pinus tabuliformis* in the park was good and was more consistent with the actual condition. However, the recognition of *Salix babylonica* and *Sabina chinensis* was unsatisfactory.

Table 5 details the confusion matrix for tree species classification of the optimal spectral band set. The table also shows that the producer accuracy of WorldView-2 tree species classification ranged from 51.48% (*Sabina chinensis*) to 85.75% (*Salix babylonica*). On the other hand, the user accuracy ranged from 47.63% (*Sabina chinensis*) to 88.48% (*Sophora japonica*). Large differences were observed in the producer and user accuracies among the various tree species and between the producer and user accuracies for the same tree species, indicating that based on image spectral information, the

classification accuracies were not ideal and require further exploration.

In this study, the spectral bands of WorldView-2 were used as signal sources, and MLC-RFE was used to analyse the importance of the eight bands in tree species classifications. The results showed the following: (1) In all band combinations, the classification that used the combination of blue and green bands displayed the lowest OA (40.9153%) and Kappa coefficient (0.3080). In all band combinations, the classification made using the set that included the near-infrared 2, red edge, yellow, red, near-infrared 1, coastal blue and green bands yielded the highest OA (74.5479%) and Kappa coefficient (0.7029). (2) In tree species classification using WorldView-2, the importance of the eight bands were sorted as follows (from important to unimportant): near-infrared 2 > red edge > yellow > red > near-infrared 1 > coastal blue > green > blue.

The results of the present study showed that different bands manifest different importances. Different band combinations produced large differences in classification accuracy, suggesting that the selection of participating bands bears importance in tree species classification. Also, participating bands should be effectively selected for tree species classification to achieve ideal results. In this study, using MLC-RFE method eliminated the unimportant spectral bands by rounds and consistently retained the most important spectral ones. Therefore, the optimal spectral band set with the highest accuracy has been obtained in this process.

MLC-RFE can select the best band combination required for image classification and reduce the dimension of the feature set. Optimal index factor (OIF) is a common selection method for the best band combination, and principal component analysis (PCA) features an important application in feature set dimension reduction. OIF is obtained through the sum of the standard deviations of all bands divided by the sum of the absolute values of the correlation coefficients between these bands. OIF was originally used to select 3 out of the n features to construct the best feature combination[18]; it was later promoted to find the optimal multiple feature combinations[19], and the best combination required for a large number of combinations $(C_n^3 + C_n^4 + \cdots + C_n^n)$. Computational and analytic processes are more complicated than MLC-RFE. In addition, MLC-RFE can sort the importance of features, whereas OIF can only find the combination of the best features. PCA uses an orthogonal transformation to convert a set of observations of possibly correlated variables into a set of values of linearly uncorrelated variables called principal components[20,21]. Then, the first few principal components with large variances are selected for classification, and the latter principal components with smaller variance are discarded as noise. In this case, information that plays an important role in classification may be lost. However, MLC-RFE need not transform the data set and eliminates the most useless features through comparison between features with a low information loss rate.

According to the results of this study, we can conclude that MLC-RFE is useful for important feature selection and can maximize classification accuracy. The approach is suitable for small urban areas, but relevant experiments on how it performs in a complex forest system remain lacking. In the future, we will use this method for high-dimension feature reduction and classification of natural complex forest systems.

1. Fassnacht, F. E. *et al.*, Review of studies on tree species classification from remotely sensed data. *Remote Sens. Environ.*, 2016, **186**(214), 64–87.
2. Ferreira, M. P. *et al.*, Mapping tree species in tropical seasonal semi-deciduous forests with hyperspectral and multispectral data. *Remote Sens. Environ.*, 2016, **179**, 66–78.
3. Li, D., Ke, Y., Gong, H. and Li, X., Object-based urban tree species classification using bi-temporal worldview-2 and worldview-3 images. *Remote Sens-(Basel)*, 2015, **7**(12), 16917–16937.
4. Heumann, B. W., An object-based classification of mangroves using a hybrid decision tree-support vector machine approach. *Remote Sens-Basel.*, 2011, **3**(11), 2440–2460.
5. Immitzer, M., Atzberger, C. and Koukal, T., Tree species classification with random forest using very high spatial resolution 8-band WorldView-2 satellite data. *Remote Sens-(Basel)*, 2012, **4**(9), 2661–2693.
6. Immitzer, M., Atzberger, C. and Koukal, T., Suitability of WorldView-2 data for tree species classification with special emphasis on the four new spectral bands. *Photogramm. Fernerkun. Geoinf.*, 2012, **5**, 573–588.
7. Pu, R. and Landry, S., A comparative analysis of high spatial resolution IKONOS and WorldView-2 imagery for mapping urban tree species. *Remote Sens. Environ.*, 2012, **124**(9), 516–533.
8. Cho, M. A. *et al.*, Mapping tree species composition in South African savannas using an integrated airborne spectral and lidar system. *Remote Sens. Environ.*, 2012, **125**(10), 214–226.
9. Peerbhay, K. Y., Mutanga, O. and Ismail, R., Investigating the capability of few strategically placed worldview-2 multispectral bands to discriminate forest species in Kwazulu-Natal, South Africa. *IEEE J. Sel. Top. Appl. Earth Obs. Remote Sens.*, 2013, **7**(1), 307–316.
10. Deng, S. *et al.*, Interpretation of forest resources at the individual tree level at purple mountain, nanjing city, china, using worldview-2 imagery by combining GPS, RS and GIS technologies. *Remote Sens-(Basel)*, 2013, **6**(1), 87–110.
11. Ghosh, A. and Joshi, P. K., A comparison of selected classification algorithms for mapping bamboo patches in lower gangetic plains using very high resolution worldview 2 imagery. *Int. J. Appl. Earth Obs. Geoinf.*, 2014, **26**(1), 298–311.
12. Guyon, I., Weston, J., Barnhill, S. and Vapnik, V., Gene selection for cancer classification using support vector machines. *Mach. Learn.*, 2002, **46**(1–3), 389–422.
13. Camps-Valls, G., Gomez-Chova, L., Calpe-Maravilla, J. and Martin-Guerrero, J. D., Robust support vector method for hyperspectral data classification and knowledge discovery. *IEEE Trans. Geosci. Remote Sens.*, 2004, **42**(7), 1530–1542.
14. Bazi, Y. and Melgani, F., Toward an optimal SVM classification system for hyperspectral remote sensing images. *IEEE Trans. Geosci. Remote Sens.*, 2006, **44**(11), 3374–3385.
15. Zhang, R. and Ma, J., A feature selection algorithm for hyperspectual data with SVM-RFE. *Geomatics Inf. Sci. Wuhan Univ.*, 2009, **34**(7), 834–837.

16. Zhang, H., Huang, B. and Yu, L., Kernel function in SVM-RFE based hyperspectral data band selection. *Remote Sens. Technol. Appl.*, 2013, **28**(5), 747–752 (in Chinese).
17. Liu, H. P., An, H. J., Wang, B. and Zhang, Q. L., Tree species classification using WorldView-2 images based on recursive texture feature elimination. *J. Beijing For. Univ.*, 2015, **37**(8), 53–59 (in Chinese).
18. Chavez, P. S., Berlin, G. L. and Sowers, L. B., Statistical method for selecting landsat MSS ratios 147. *J. Appl. Photogr. Eng.*, 1982, **8**(1), 23–30.
19. Qaid, A. M. and Basavarajappa, H. T., Application of optimum index factor technique to landsat7 data for geological mapping of north east of Hajjah, Yemen. *Am.-Eurasian J. Sci. Res.*, 2008, **3**(1), 84–91.
20. Malhi, A. and Gao, R. X., PCA-based feature selection scheme for machine defect classification. *IEEE Trans. Instrum. Meas.*, 2004, **53**(6), 1517–1525.
21. Kumaran, N. and Bhavani, R., PCA-based feature selection for MRI image retrieval system using texture features. *Artif. Intell. Evol. Algorithms Eng. Syst.*, Springer India, 2015, **324**, 109–117.

ACKNOWLEDGEMENTS. This work was supported by the National Nature Science Foundation of China (grant no. 61502219) and the International Science and Technology Cooperation Program of China (grant no. 2016YFE0104600). We expres our gratitude to the editors and anonymous reviewers.

Received 30 August 2017; revised accepted 15 June 2018

doi: 10.18520/cs/v115/i7/1366-1374

Effect of humic acid application rates on physicochemical and fertility properties of sandy loam soil grown with mung bean under different irrigation water regimes

Abdulmohsin R. Al-Shareef[1], Saleh M. Ismail[2,*] and Fathy S. El-Nakhlawy[2]

[1]Ge. GIS Applied Department, and
[2]Arid Land Agriculture Department, Faculty of Meteorology, Environment and Arid Land Agriculture, King Abdulaziz University, Jeddah, Saudi Arabia

A field experiment was carried out to evaluate the changes in some physicochemical and fertility properties of sandy loam soil treated with three different rates of humic acid (HA) under three different irrigation water regimes. Soil bulk density and saturated hydraulic conductivity were decreased while organic matter was increased by increasing HA rates. Decreasing water regime and increasing HA rate increased soil salinity. Decreasing irrigation water regime increased nitrogen and reduced available phosphorus and potassium. Increasing HA rate increased nitrogen and available phosphorus and potassium.

Keywords: Drip irrigation, macro-nutrients, soil properties, water stress.

CULTIVATING sandy and sandy loam soils to mitigate the global food problems using least amount of irrigation water and mineral fertilizers is greatly required and recommended[1]. Also, water stress is considered to be one of the major problems in global agricultural production which leads to a huge decrease in crop yield especially in arid and semiarid regions, where there is not enough rain[2].

Based on previous studies, humic acid (HA) which is considered a vital constituent and a friendly part of soil organic structure was used to conserve water in root-zone area[3,4]. Therefore, water availability increases due to reduced run-off and deep percolation that ultimately increases crop yield. Moreover, application of HA helps to improve soil physical and chemical properties, i.e. water retention, permeability, water infiltration, drainage, aeration, structure and nutrient availability. As a result, water usage was reduced[3,4] in sandy loam soil using 10 kg ha^{-1} of granular HA which decreased soil bulk density (BD) and saturated hydraulic conductivity (SHC) while increasing water holding capacity, soil organic matter and soil nutrients under fully and water stress conditions[5]. Beside containing nutrients, humic substances can chelate soil nutrients and improve nutrient uptake, especially phosphorus, sulphur, nitrogen and zinc because they act as a sink for such nutrients[6–9].

In arid regions, water resources are limited and the majority of cultivated land contains light textured soils (sandy and sandy loam). Using HA as a soil amendment could be a practical option to increase water and fertilizer efficiencies. Therefore, the present study was aimed at evaluating changes in soil organic matter, soil bulk density, saturated hydraulic conductivity, soil pH, soil salinity, total nitrogen and available phosphorus and potassium of sandy loam soil treated with different rates of HA under different irrigation water regimes.

A field experiment was carried out for two consecutive seasons of 2015–2017 at the Agriculture Research Station of King Abdulaziz University located at Hada Al-Sham, 110 km northeast of Jeddah, KSA. The soil texture of the experimental site was classified as sandy loam. The design of the experiment was a split plot with four replications. The plot size was 6 m^2 (2 m × 3 m). The main plots comprised three irrigation water regimes. The first represented full irrigation (100%) water requirement (WR). The second and third were 80% and 60% of the first regime, and represented stress treatments. The full irrigation water requirement was calculated based on the

*For correspondence. (e-mail: smii2001@gmail/com)